Broadband Permittivity and Loss Tangent Measurements using a Split-Cylinder Resonator*

Michael D. Janezic†, Edward F. Kuester‡ and James Baker-Jarvis†

†National Institute of Standards and Technology, Boulder, Colorado 80305, USA
‡University of Colorado, Boulder, Colorado 80309, USA

Abstract

We summarize a theoretical model for the split-cylinder resonator, based on the mode-matching method, for nondestructively measuring permittivity and loss tangent with the split-cylinder resonator. This new model correctly accounts for the fringing electric and magnetic fields, thereby improving the measurement accuracy of the technique. Previously, the split-cylinder resonator has been used for single-frequency permittivity and loss tangent measurements using only the fundamental TE_{011} resonant mode. Using higher-order TE_{0np} modes, we demonstrated how to measure the permittivity and loss tangent of dielectric substrates over an extended frequency range. We validated the new model by measuring the permittivity and loss tangent from 10 to 50 GHz of fused-silica substrates and compared them with measurement data obtained with a circular-cylindrical cavity, a dielectric-post resonator, and several split-post resonators.

INTRODUCTION

The split-cylinder resonator technique is a nondestructive method for measuring the permittivity and loss tangent of low-loss dielectric substrates. Originally proposed by Kent [1, 2], this method employs a circular-cylindrical cavity, that is separated into two halves, as shown in Fig. 1. A sample is placed in the gap between the two shorted cylindrical waveguide sections. A coupling loop in each waveguide section excites a TE_{0np} resonance, and from measurements of the resonant frequency and quality factor, the permittivity and loss tangent of the sample can be determined.

The advantage of the split-cylinder method is that the sample needs only to be planar and extend sufficiently far beyond the diameter of the two cylindrical waveguide sections. No other sample machining is necessary, making this method attractive for accurate, nondestructive measurements of low-loss substrates. Unfortunately, having little or no sample preparation comes at the cost of needing a more complicated theoretical model. For the case of the split-cylinder, the model must include the electric and magnetic fields that extend into the sample region beyond the cylindrical waveguide regions. In order to obtain accurate measurements of permittivity and loss tangent, these fields must be accurately determined.

Previously [3], we developed a theoretical model employing Hankel transforms that rigorously accounted for these fringing fields and improved the accuracy of the permittivity measurements. From this theoretical model, we derived a resonance condition for the split-cylinder resonator, which allowed us to calculate the sample permittivity. Although accurate, this new model was computationally intensive, so we have developed a new theoretical model for the split-cylinder resonator, based on the mode-matching method. Using this model, we derived equations for calculating the relative permittivity and loss tangent of a sample. We summarize this new theoretical model and show how to use the resulting equations to calculate the sample permittivity and loss tangent.

In the past, only the fundamental TE_{011} resonant mode of the split-cylinder resonator has been used to measure the permittivity and loss tangent. However, the mode-matching model we present is valid also for higher-order TE_{0np} resonant modes. From measurements of the TE_{0np} resonant frequency and quality factor, we show how to calculate the relative permittivity and loss tangent of the substrate under test over a frequency range of 10 to 50 GHz. In order to ver-

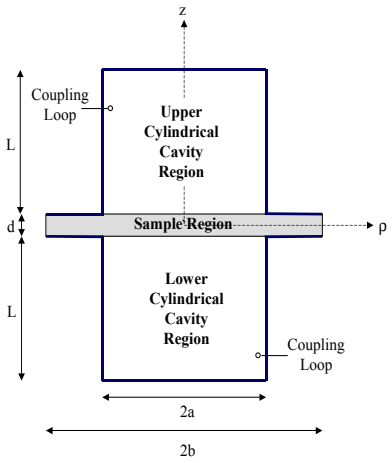

Figure 1: Cross-sectional diagram of a split-cylinder resonator.

ify the accuracy of these measurements, we compared measurements on fused-silica substrates using a split-cylinder resonator to measurement data obtained with a circular-cylindrical cavity, dielectric-post resonator, and several split-post resonators.

RELATIVE PERMITTIVITY

In our initial model for calculating the sample permittivity, we assumed that the sample extended to infinity in the radial direction [3]. However, if the fringing electric and magnetic fields decrease as a function of ρ in the sample region, we may assume that a perfect conductor exists at some sufficiently large radius $\rho = b$, without introducing a systematic error in the calculation of the sample permittivity and loss tangent. By introducing this boundary, we enclose the entire split-cylinder resonator fixture, and derive a new model based on the mode-matching method.

Assuming TE_{0n} mode excitation, we determined the transverse electric and magnetic fields in the upper cylindrical-cavity region from Maxwell's equations with enforcement of the boundary conditions on the upper waveguide endplate and walls:

$$E_{\phi_u}(\rho,z) = \sum_{n=1}^{N_u} A_n U_n J_1(h_{n_u}\rho)\sin\left[p_{n_u}(L+\frac{d}{2}-z)\right], \quad (1)$$

$$H_{\rho_u}(\rho,z) = -\frac{1}{j\omega\mu_0}\sum_{n=1}^{N_u} A_n U_n p_{n_u} J_1(h_{n_u}\rho)\cos\left[p_{n_u}(L+\frac{d}{2}-z)\right], \quad (2)$$

where $p_{n_u}^2 = k_u^2 - h_{n_u}^2$, $k_u^2 = \omega^2\mu_0\epsilon_0\epsilon_a^{'}$, $h_{n_u} = \frac{j_{1,n}}{a}$, A_n are constants to be determined, and N_u is the total number of modes included in the upper cylindrical-cavity region. Additional geometrical parameters are given in Fig. 1. To improve matrix conditioning we have included the factors $U_n = p_{N_u}/\cosh\left[\mathrm{Im}(p_{n_u})L\right]$.

Since the sample region is also enclosed by a perfect conductor at $\rho = b$, we similarly express the transverse electric and magnetic fields in the sample region:

$$E_{\phi_s}(\rho,z) = \sum_{n=1}^{N_s} B_n V_n J_1(h_{n_s}\rho)\cos\left(p_{n_s}z\right), \quad (3)$$

$$H_{\rho_s}(\rho,z) = -\frac{1}{j\omega\mu_0}\sum_{n=1}^{N_s} B_n V_n p_{n_s} J_1(h_{n_s}\rho)\sin\left(p_{n_s}z\right), \quad (4)$$

where $p_{n_s}^2 = k_s^2 - h_{n_s}^2$, $k_s^2 = \omega^2\mu_0\epsilon_0\epsilon_s^{'}$, $h_{n_s} = \frac{j_{1,n}}{b}$, B_n are constants to be determined, and N_s is the total number of modes included in the sample region. In this case, we included the terms $V_n = p_{N_s}/\cosh\left[\mathrm{Im}(p_{n_s})\frac{d}{2}\right]$ to improve matrix conditioning.

We derive a resonance condition by enforcing the boundary conditions for the transverse electric and magnetic field. The tangential electric and magnetic fields are continuous at $z = d/2$:

$$E_{\phi_u}\left(z=\frac{d}{2}\right) = E_{\phi_s}\left(z=\frac{d}{2}\right) \quad 0\le\rho\le b, \quad (5)$$

$$H_{\rho_u}\left(z=\frac{d}{2}\right) = H_{\rho_s}\left(z=\frac{d}{2}\right) \quad 0\le\rho\le a. \quad (6)$$

Substituting the series electric and magnetic field expressions (1-4) into (5) and (6), multiplying each side by the electric or magnetic field [H_{ρ_s} in the case of (5), E_{ϕ_u} in the case of (6)], integrating over the appropriate cross-section, and employing orthogonality of the modes [4], we obtain two systems of equations:

$$\mathbf{QA} = \mathbf{RB} \quad (7)$$

and

$$\mathbf{SA} = \mathbf{PB}, \quad (8)$$

where

$$Q_{mn} = A_n U_n \frac{a h_{nu}}{h_{ms}^2 - h_{nu}^2} J_1(h_{ms}a) J_0(h_{nu}a)\sin(p_{nu}L), \quad (9)$$

$$R_{mm} = B_m V_m \frac{b^2}{2} J_0^2(h_{ms}b)\cos(p_{ms}\frac{d}{2}), \quad (10)$$

$$S_{nn} = A_n U_n p_{nu}\frac{a^2}{2} J_0^2(h_{nu}a)\cos(p_{nu}L), \quad (11)$$

and

$$P_{nm} = B_n V_m p_{Ns}\frac{a p_{ms} h_{nu}}{h_{ms}^2 - h_{nu}^2} J_1(h_{ms}a) J_0(h_{nu}a)\sin(p_{ms}\frac{d}{2}). \quad (12)$$

Note that both $\mathbf{R}$ and $\mathbf{S}$ are diagonal matrices.

The system of equations represented by (7) and (8) is rewritten as

$$[\mathbf{Z}][\mathbf{X}] = \mathbf{0}, \tag{13}$$

where

$$[\mathbf{Z}] = \begin{bmatrix} \mathbf{Q} & -\mathbf{R} \\ \mathbf{S} & -\mathbf{P} \end{bmatrix} \tag{14}$$

and

$$[\mathbf{X}] = \begin{bmatrix} \mathbf{A} \\ \mathbf{B} \end{bmatrix}. \tag{15}$$

The resonance condition follows from the fact that this linear system of equations has a nontrivial solution only if

$$\det[\mathbf{Z}] = 0. \tag{16}$$

We can use (16) to iteratively calculate either the resonant frequency of the split-cylinder cavity given a known sample permittivity $\epsilon_s^{'}$, or the sample permittivity given a measured resonant frequency f.

LOSS TANGENT

In order to discuss the measurement of the sample loss tangent $\tan\delta_s$, we must first examine the definition of the measured quality factor Q of the split-cylinder resonator when a sample is present:

$$Q = \frac{\omega(W_a + W_s)}{P_e + P_f + P_w + P_s}, \tag{17}$$

where W_a and W_s are the average energies stored in the cylindrical cavity and sample regions, and P_w, P_c, P_f, and P_s are the powers dissipated per second in the cylindrical cavity endplate, walls, flange, and sample respectively. Note that we have ignored the power dissipated in the coupling loops because we ensured that the resonance was very weakly coupled (<-50 db). When we calculate the sample permittivity using (16), we also determine the coefficients A_n and B_n, thereby allowing us to write the energy-stored terms as

$$W_s = \epsilon_0\epsilon_s^{'} \int_{z=0}^{\frac{d}{2}} \int_{\rho=0}^{b} \int_{\phi=0}^{2\pi} |E_{\phi_s}|^2 \rho \; d\phi \, d\rho \, dz, \tag{18}$$

$$W_a = \epsilon_0\epsilon_a^{'} \int_{z=\frac{d}{2}}^{L} \int_{\rho=0}^{a} \int_{\phi=0}^{2\pi} |E_{\phi_u}|^2 \rho \; d\phi \, d\rho \, dz, \tag{19}$$

and the power-dissipation terms as

$$P_e = R_s \int_{\rho=0}^{a} \int_{\phi=0}^{2\pi} |H_{\rho_u}|^2 \rho \; d\phi \, d\rho \, \Big|_{z=L}, \tag{20}$$

$$P_w = R_s \int_{z=\frac{d}{2}}^{L} \int_{\phi=0}^{2\pi} |H_{z_u}|^2 \rho \; d\phi \, dz \, \Big|_{\rho=a}, \tag{21}$$

$$P_f = R_s \int_{\rho=a}^{b} \int_{\phi=0}^{2\pi} |H_{\rho_s}|^2 \rho \; d\phi \, d\rho \, \Big|_{z=\frac{d}{2}}, \tag{22}$$

$$P_s = \tan\delta \, \omega\epsilon_0\epsilon_s^{'} \int_{\rho=0}^{b} \int_{z=0}^{\frac{d}{2}} \int_{\phi=0}^{2\pi} |E_{\phi_s}|^2 \rho \; d\phi \, d\rho \, dz. \tag{23}$$

Given that $\epsilon_s^{'}$ is calculated from the measured resonant frequency, the two remaining unknown variables used to determine the energy stored and power dissipated are the surface resistivity R_s of the cylindrical waveguide sections and the loss tangent $\tan\delta$ of the sample. We obtain R_s from a measurement of the quality factor of the empty split-cylinder resonator, where the gap between the cylindrical waveguide sections is closed. Then, after measuring the quality factor Q of the split-cylinder when the sample is present, we solve (17) for the sample loss tangent $\tan\delta$.

MEASUREMENT RESULTS

We used two split-cylinder resonators to measure the complex permittivity of two fused-silica substrates over a frequency range of 10 to 50 GHz. The first split-cylinder resonator, whose TE_{011} resonant frequency is 10 GHz with no sample, had dimensions $2a$=38.1 mm and L=25.3 mm. The resonator was constructed from oxygen-free copper and had a small hole in the waveguide wall for the coupling loop. The second split-cylinder resonator, whose TE_{011} resonant frequency is 35 GHz with no sample, had dimensions $2a$=13.18 mm and L=3.51 mm. The resonator was constructed from silver-plated brass and also had small holes in each section to accommodate the coupling loops.

Two fused-silica samples machined from the same lot were measured with the two split-cylinder resonators. The sample for the larger split-cylinder resonator was 55 mm square and 0.81 mm thick. The sample for the smaller resonator was 25 mm square and 0.28 mm thick. Each sample was placed between the two waveguide sections of the split-cylinder resonator, and the resonance curve for the TE_{011} mode was examined on an automatic network analyzer. From the resonance curve, we obtained the resonance frequency f and the quality factor Q. From these two quantities and the geometrical dimensions of the split-cylinder resonator and sample, we calculated the sample relative permittivity using (16) and the sample loss tangent using (17).

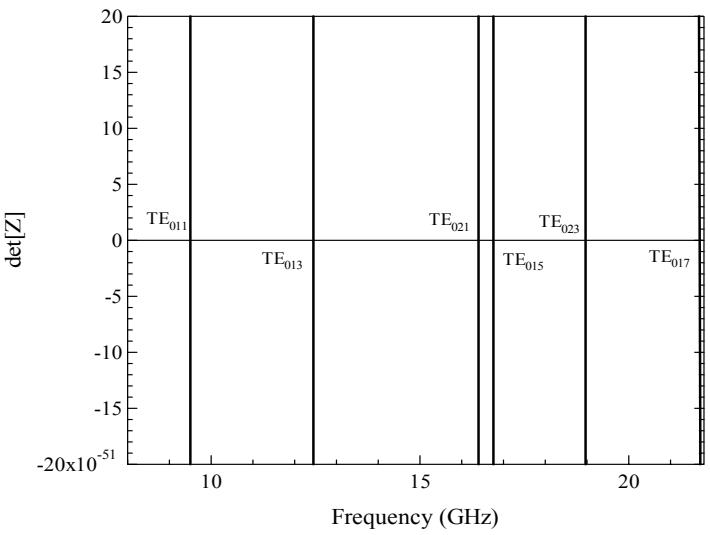

Figure 2: Zero-crossings of det[**Z**] showing the frequencies of the first six TE_{0np} resonant modes.

We noted earlier that equation (16) could be used to calculate the resonant frequency of the split-cylinder resonator, given the substrate's relative permittivity and thickness and the dimensions of the split-cylinder resonator. Using the value of the relative permittivity calculated from the TE_{011} resonance, we plotted det[**Z**] as a function of frequency as shown in Figure 2. The first zero crossing corresponds with the TE_{011} mode while the other zero crossings correspond to the higher-order TE_{0np} modes. It is important to note where these frequencies occur before attempting to measure them with a network analyzer because as the frequency increases, modes other than those in the TE_{0np} family are excited. Using the information contained in Figure 2 reduces the chance of measuring an incorrect mode.

After correctly identifying the higher-order modes, we measured the resonant frequency and quality factor of each using a network analyzer. In some cases, the TE_{0np} mode may be close in frequency to other resonant modes, distorting the resonance curve. One must use these modes with caution as this distortion may cause errors in the calculation of the resonant frequency and quality factor. Once the resonant frequency and quality factor are accurately measured, we again calculate the relative permittivity and loss tangent of the substrate using (16) and (17). Figure 3 shows the measured relative permittivity of fused silica using two split-cylinder resonators. As expected, the permittivity is relatively flat over the frequency range. Figure 4 shows the measured loss tangent of fused silica measured with the two split-cylinder resonators. We noted an increase in the loss tangent as a function of frequency and when we performed a least squares fit to the data, we found the increase in the loss tangent to be linear over the frequency range of 10 to 50 GHz.

Finally, to verify the accuracy of the measurements on fused silica, we machined additional samples for testing in a circular-cylindrical cavity, a dielectric-post resonator, and several split-post resonators. In Figures 5 and 6 we compare our split-cylinder resonator measurements of relative permittivity and loss tangent to measurements made using these other methods. We found very good agreement between all the methods for both relative permittivity and loss tangent over the frequency range from 1 to 50 GHz.

CONCLUSIONS

Using the mode-matching method, we developed a theoretical model for the split-cylinder resonator method. The model includes not only the TE_{011} resonant mode, but also the higher-order TE_{0np} modes that occur at higher frequencies. Using measurements of the resonant frequencies and quality factors of the higher-order TE_{0np} modes, we accurately measured the relative permittivity and loss tangent of fused silica over a frequency range of 10 to 50 GHz and found them to agree with measurements made in a circular-cylindrical cavity, dielectric-post resonator, and several split-post resonators.

REFERENCES

[1] G. Kent, "An evanescent-mode tester for ceramic dielectric substrates," *IEEE Trans. Microwave Theory Tech.*, vol. 36, no. 10, pp. 1451–1454, October 1988.

[2] G. Kent and S. Bell, "The gap correction for the resonant-mode dielectrometer," *IEEE Trans. Instrum. Meas.*, vol. 45, no. 1, pp. 98–101, February 1996.

[3] M.D. Janezic and J. Baker-Jarvis, "Full-wave analysis of a split-cylinder resonator for nondestructive permittivity measurements," *IEEE Trans. Microwave Theory Tech.*, vol. 47, no. 10, pp. 2014–2020, October 1999.

[4] A.S. Omar G.V. Eleftheriades and L.P.B. Katehi, "Some important properties of waveguide junction generalized scattering matrices in the context of the mode matching method," *IEEE Trans. Microwave Theory Tech.*, vol. 42, pp. 1896–1903, October 1994.

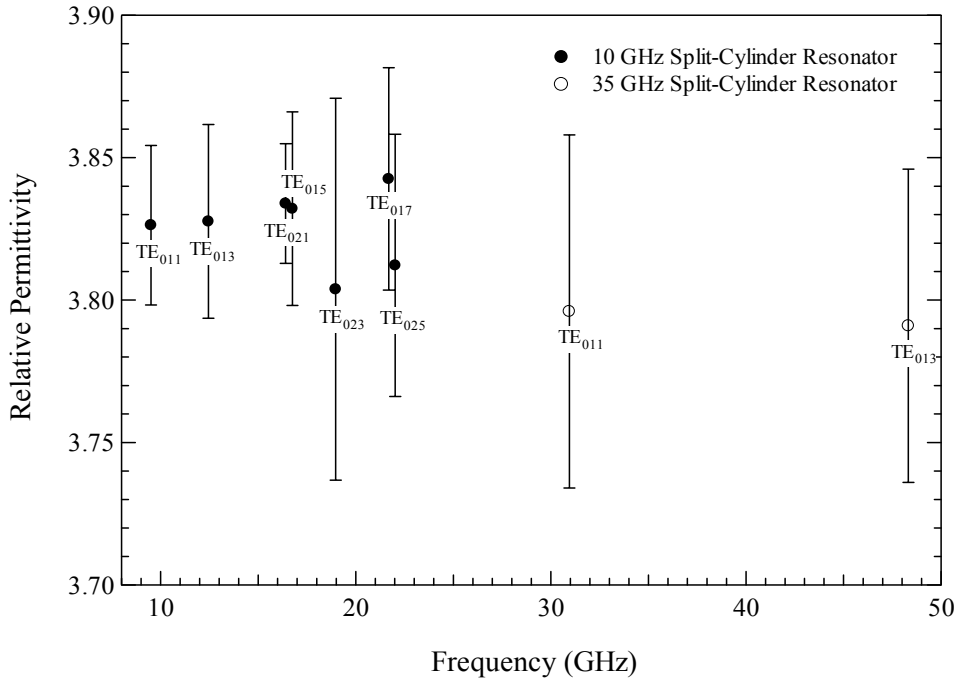

Figure 3: Relative permittivity measurements of fused silica using several split-cylinder resonator modes.

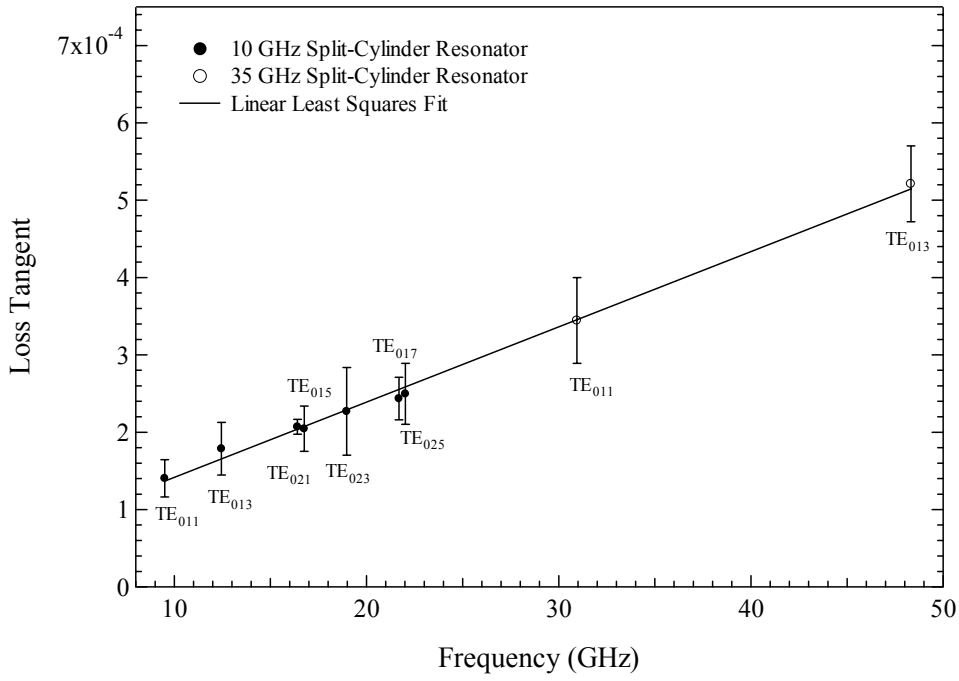

Figure 4: Loss tangent measurements of fused silica using several split-cylinder resonator modes.

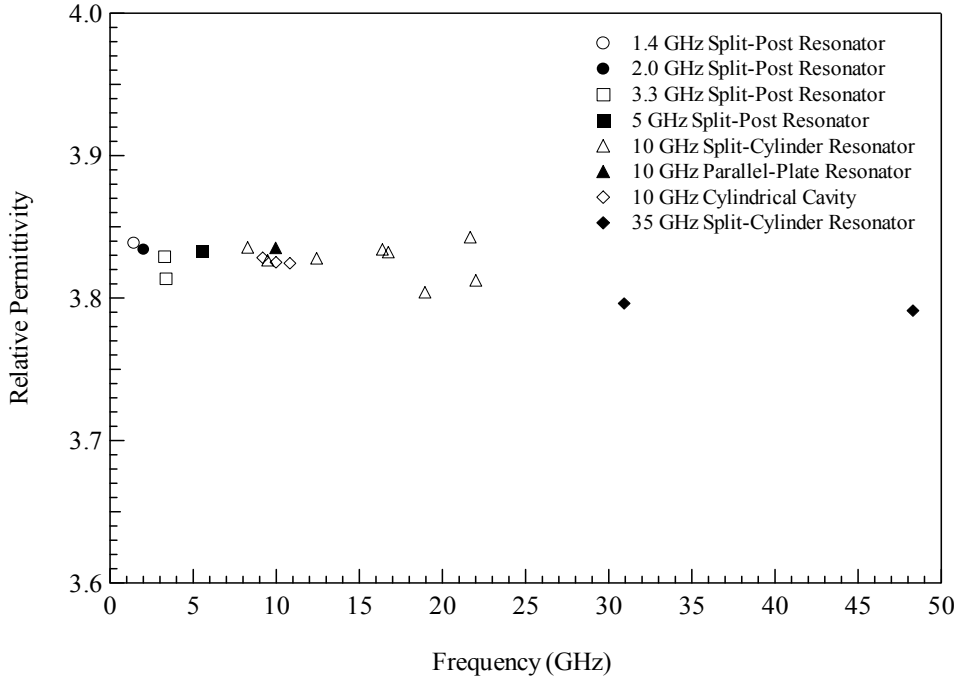

Figure 5: Broadband relative permittivity measurements of fused silica using various measurement methods.

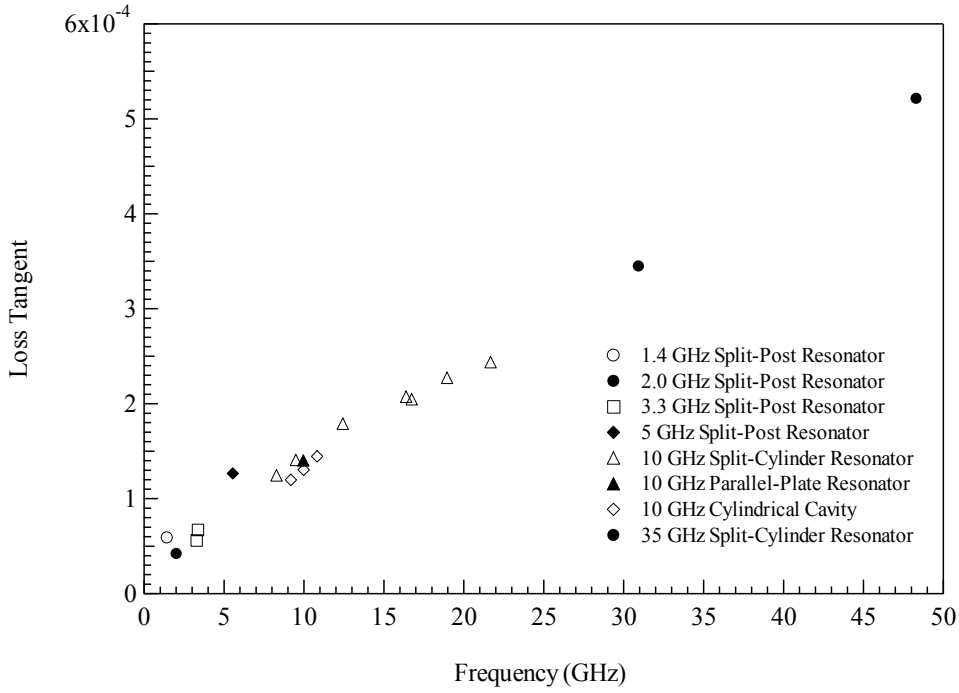

Figure 6: Broadband loss tangent measurements of fused silica using various measurement methods.